Behavioral/Cognitive

Spatial Frequency Tuning Follows Scale Invariance in the Human Visual Cortex

Emily Wiecek,[1,2,3] Luis D. Ramirez,[3,5] Michaela Klimova,[3,4] and Sam Ling[3]
[1]Boston Children's Hospital, Boston, Massachusetts 02115, [2]Harvard Medical School, Boston, Massachusetts 02115, [3]Boston University, Boston, Massachusetts 02115, [4]Northeastern University, Boston, Massachusetts 02115, and [5]University of California San Diego, La Jolla, California 92093

Our visual system can recognize patterns across many spatial scales. A fundamental assumption in visual neuroscience is that this ability relies on the putative scale-invariant properties of receptive fields (RFs) in early vision, whereby the spatial area over which a visual neuron responds is proportional to the spatial scale of information it can encode (i.e., spatial frequency, SF). In other words, the resolution of spatial sampling of a RF is assumed to be constant in the visual cortex. However, this assumption has gone untested in the human visual cortex. To address this, we leveraged model-based fMRI techniques that characterize the spatial tuning and SF preferences of cortical subpopulations sampled within a voxel across eight participants (five females, three males). We find that the voxel-wise ratio between peak SF tuning and RF size—expressed as "cycles per RF"—remains constant across visual areas V1, V2, and V3, suggesting that, at the population level, SF preferences are inversely proportional to the RF size, a tenet of scale invariance in early human vision.

Key words: **neuroimaging; receptive fields; spatial vision; visual cortex**

Significance Statement

The human visual system interprets patterns across a range of spatial scales, a capability thought to rely on scale-invariant properties of receptive fields (RFs). Although widely assumed, this principle had not been directly tested in the human brain. Using model-based fMRI, we measured how the population RF size and spatial frequency (SF) tuning vary across the visual field. We use a novel metric, cycles per RF, to reveal that SF preferences scale inversely with the RF size across early visual areas (V1–V3). This provides the first direct evidence of scale invariance in the human visual cortex and offers a new framework for characterizing how spatial information is sampled and represented in early vision.

Introduction

Scale invariance is a ubiquitous property in nature wherein patterns persist across the spatial scales of a system; from fractals in snowflake crystals to the clustering of galaxies, simple rules can generate complex yet stable patterns. In visual neuroscience, scale invariance refers to the idea that the visual system can recognize and discriminate patterns across different spatial scales, for example, recognizing the same object independent of the retinal image's size or eccentricity. Psychophysical and physiological evidence suggest that scale invariance in vision is mediated by interacting factors such as the changing density and size of receptive fields (RFs) across the visual field and how spatial information is consequently pooled by neurons along the early visual cortex (Jamar and Koenderink, 1983). To elaborate, the spatial area over which a visual neuron responds (its RF size) is inversely proportional to the scale of spatial information (spatial frequency, SF) it is tuned to encode (Teichert et al., 2007). This relationship is believed to compensate for the cortical magnification factor, wherein more cortices are dedicated to representing central versus peripheral vision (Wiskott, 2006; Teichert et al., 2007). Put together, the effective resolution of spatial sampling performed by RFs is thought to remain roughly constant across the visual field, despite differences in retinal sampling and cortical representation. However, this has not been directly tested at the population level, particularly in humans.

Recent advances in functional neuroimaging have enabled the detailed study of spatial processing across the early visual cortex. Population RF (pRF) mapping characterizes the spatial area to which the neural population sampled within a voxel will respond (Dumoulin and Wandell, 2008), while population SF tuning (pSFT) describes the scale at which that spatial information is processed (Aghajari et al., 2020). Additionally, both pRF and pSFT have a reproducible relationship with eccentricity that is

Received July 31, 2025; revised Dec. 5, 2025; accepted Dec. 20, 2025.
Author contributions: E.W. and S.L. designed research; E.W., L.D.R., and M.K. performed research; L.D.R. and S.L. contributed unpublished reagents/analytic tools; E.W. analyzed data; E.W., L.D.R., M.K., and S.L. wrote the paper.
This work was supported by the National Eye Institute (K23EY034212 to E.W. and EY028163 to S.L.). We thank Minsun Park for the helpful feedback.
The authors declare no competing financial interests.
Correspondence should be addressed to Emily Wiecek at Emily.wiecek@childrens.harvard.edu.
This paper contains supplemental material available at: https://doi.org/10.1523/JNEUROSCI.1490-25.2025
https://doi.org/10.1523/JNEUROSCI.1490-25.2025

corroborated by both physiological and neuroimaging studies: the pRF size increases, and preferred SF decreases with increasing eccentricity (Van Essen et al., 1984; Dumoulin and Wandell, 2008). Using these two computational neuroimaging approaches, pRF and pSFT, we set out to test the theory of scale invariance in the early visual cortex. Under scale invariance, the RF size and SF tuning vary inversely to maintain a constant resolution of spatial encoding within the RF. This relationship has motivated the use of a cortical magnification factor to adjust the size of visual stimuli and equate performance between central and peripheral vision in both psychophysical and neuroimaging vision research (Rovamo and Virsu, 1979). However, cortical magnification is commonly derived from the anatomical surface area and does not directly capture the functional sampling properties measurable by neuronal pRFs. Specifically, recent work has highlighted that cortical magnification alone cannot fully account for variance in spatial tuning, suggesting a need to consider functional measures (Silva et al., 2018; Benson et al., 2021).

Here, we leverage pRF and pSFT estimates to directly test scale invariance in the early visual cortex. Unlike cortical magnification, the pRF size provides an empirically measured index of spatial sampling. We formalize spatial sampling with a new, unitless metric, cycles per RF (CPF) that extends beyond anatomical magnification, enabling us to characterize how finely a pRF samples space relative to its size and test whether this sampling is indeed constant across the visual field.

Materials and Methods

Participants. Eight healthy, typically sighted volunteers [five females, three males, median age 28 (range 21–33)] participated in two 2 h neuroimaging sessions for this study (the first mapped pRFs, pRF, and the second pSFT). All participants were correctable to 20/20 vision in each eye and wore any required refractive correction during all neuroimaging sessions. All participants signed an informed consent before participation in the study and were reimbursed for their time. Study procedures were approved by the Boston University Institutional Review Board.

Functional magnetic resonance imaging data acquisition and preprocessing. All MRI data were collected on a Siemens 3 T Prisma scanner at the Boston University Cognitive Neuroimaging Center using a 64-channel head coil (Siemens Healthcare). Each participant had a whole-brain anatomical scan with T1-weighted multiecho magnetization prepared rapid gradient echo sequence [1.0 mm^3; FOV, $192 \times 192 \times 176$; fractional anisotropy flip angle (FA), 7°; TR, 2,200 ms; TE, 1.57 ms; TI, 1,100 ms; van der Kouwe et al., 2008]. For each functional scanning session, blood oxygen level-dependent (BOLD) activity was measured with T_2*-weighted in-plane echoplanar imaging (EPI) pulse sequence with simultaneous multislice (SMS) imaging and a field of view perpendicular to the calcarine sulcus (2 mm^3 voxels; FOV, $936 \times 936 \times 330$ mm; FA, 64°; TR, 1,000 ms; TE, 30 ms). BOLD data for the pRF mapping session were acquired with the following parameters: 2 mm^3 voxels; FOV, $60 \times 112 \times 172$ mm; FA, 80°; TR, 1,000 ms; TE, 35 ms (Moeller et al., 2010; Xu et al., 2013); and multiband acceleration factor, 5. The University of Minnesota's CMRR-MB pulse sequence was used for SMS-EPI acquisition.

For both pRF and pSFT scanning sessions, stimuli were presented and displayed using a linearized VPixx PROPixx projector (DLP LED; resolution, $1,024 \times 768$ pixels; refresh rate, 60 Hz; viewing distance, ~99 cm). Gaze position was monitored at a sampling rate of 500 Hz with an MRI-comparable EyeLink 1000 Plus infrared eye tracker (SR Research). Each scan began with an eight-point eye calibration. A bivariate ellipse contour area (BCEA) was calculated for each subject as a measure of fixation stability for both the pRF and pSFT scanning sessions. Supplementary Figure 1 shows BCEA across subjects. Median fixation stability was 0.99^{o2} for pRF and 1.0^{o2} for pSFT (paired Wilcoxon rank test, $p = 1.0$).

Prior to fMRI analysis, functional data were corrected for EPI distortion using reverse-phase encoding in FSL and then preprocessed with FreeSurfer's FS-FAST using standard motion correction and slice timing correction procedures and temporally high-pass filtered (cutoff, 0.01 Hz) to remove any low-frequency drift (Andersson et al., 2003). For each functional run, we converted the raw MR signal to units of percent signal change by dividing each voxel by its mean intensity across that run. To optimize for voxel-wise analyses, no volumetric spatial smoothing was performed and voxel-wise estimates for separate scanning sessions were aligned using FreeSurfer's boundary-based registration (Greve and Fischl, 2009). All subjects observed both pRF and pSFT stimuli monocularly, alternating occlusion before each run (five runs total for each eye for both pRF and pSFT). Monocular viewing was done to serve as control data for a concurrent study. For the purposes of this study, data across all 10 runs for both pSFT and pRF were concatenated and analyzed as a single scanning session.

Visual stimuli and procedures: pRF mapping. All visual stimuli were generated with MATLAB using the Psychophysics Toolbox-3 (Brainard, 1997). pRF was used to determine voxel-wise retinotopic preferences and to delineate regions of interest (ROIs) for cortical areas V1–V3 using standard techniques and stimuli (Dumoulin and Wandell, 2008; Kay et al., 2013). We focused our analyses on V1–V3 because reliable boundaries can be defined in these regions based on polar angle preference, and pSFT has not been validated past area V3 (Aghajari et al., 2020). pRF data analysis was performed using the analyzepRF MATLAB toolbox, which estimated the visual field eccentricity, polar angle, and RF size for every voxel within the cortical ribbon of the occipital lobe (Dumoulin and Wandell, 2008; Kay et al., 2013). The RF size (sigma) was estimated using the size and exponent estimates from the compressive spatial summation model (Kay et al., 2013). Supplementary Figure 2 depicts RF size estimates with the compressive exponent. Each pRF session involved 3–5 scans of both rotating wedge stimuli and bar sweep and expanding/contracting ring stimuli. Participants were asked to maintain central fixation during stimulus presentation and report a color change by pressing a button when the fixation dot changed from red to white or white to red. Stimuli consisted of colored objects and faces of varying sizes over a pink noise background and were presented on a uniform gray background (mean luminance ~150 cd/m^2). Each participant completed three bar runs and two wedge runs for each eye in a 2 h scanning session. All 10 monocular runs (five from each eye) were concatenated for pRF fitting.

Visual stimuli and procedures: pSFT. Voxel-wise pSFT was acquired using procedures similarly described in Aghajari et al. (2020). During a scanning session, participants viewed bandpass filtered uniformly distributed noise, with peak SF ranging from 0.5 to 12 cycles per degree (cpd). The filter width was fixed at 0.2 cpd. Ten unique noise samples were generated for each of the 40 logarithmically sampled SFs. Each SF was presented for 1 s and at a 10 Hz noise sample refresh rate. Stimuli had a Michelson contrast of 100% and a diameter of 17°. A fixation point was presented as a 0.15° circle in the center of the screen surrounded by a 0.32° Gaussian annulus. The luminance of the fixation point changed pseudorandomly from 0 (black) to 60 (gray) in 8 bit grayscale units (range 0–255), and participants reported this change with a button press. Presentation of the stimuli started and ended with a 10 s blank fixation period on a mid-luminance background. Each participant completed a total number of 10 runs (five runs presented monocularly to each eye), in a 2 h scanning session separate from pRF mapping.

Model-based estimation for pSFT. Estimates for voxel-wise preferred SF and tuning bandwidth were calculated as described in (Aghajari et al., 2020). In summary, we presume that the BOLD response to a series of presented SFs can be modeled with a log Gaussian distribution (Eq. 1) as follows:

$$R([f(t)]) = e^{-\frac{[\log(f(t)) - \log(\mu)]^2}{2\sigma^2}}, \quad (1)$$

where μ (peak) and σ (tuning bandwidth) are both free parameters and f is the SF displayed at time t. Because SF mapping stimuli were not

presented during the blank periods in between blocks, the SF input during blank periods was set to 0.0001 cpd to avoid taking the log-transform of 0. We then convolve the predicted response with a standard hemodynamic response function (Eq. 2) to calculate a predicted BOLD response (Eq. 3) as follows:

$$h(t) = \frac{(t/\tau)^{(n-1)} e^{-(t/\tau)}}{\tau(n-1)!}, \quad (2)$$

where τ is a fixed time constant (1.08), n is the phase delay (fixed at 3), and t is the delay between stimulus onset and the BOLD response (fixed at 2.05) as follows:

$$B(t) = \beta_0 + \beta \cdot R(f[t]) * h(t), \quad (3)$$

where β_0 represents the baseline and β represents a scaling coefficient for the BOLD percent signal change. We then used fmincon to search for optimal values for μ, σ, β, and β_0 with nonlinear regression to minimize the sum-of-squares error (SSE) between the predicted and measured BOLD signal.

To optimize the nonlinear regression analysis, we performed two preliminary grid searches to identify starting values for both μ and σ. The first coarse grid search used 10 logarithmically spaced μ values and 10 linearly spaced σ values. The combination of values that resulted in the lowest SSE was used to generate a second set of values for the fine-grid search. Here, 100 logarithmically spaced values for μ and 100 linearly spaced values for σ were implemented to find the combination that resulted in the lowest SSE. The values obtained were used as the initial values for nonlinear regression. During regression analysis, values were constrained based on previous work, where μ values fell between 0.009 and 6, σ values between 0.1 and 4, β_0 values between −10 and 10, and β values between −25 and 25 (Aghajari et al., 2020). The coefficient of determination, R^2, between the predicted and measured BOLD signal was used to assess the goodness of fit and subsequent voxel selection.

Voxel selection. pRF and pSFT estimates were used to select voxels for subsequent analysis. For pRF parameters, we excluded any voxel with an R^2 lower than 10% and a pRF size less than 0.1° in diameter. From this pool, we included voxels that had an eccentricity between 0.2 and 8.5°. These eccentricity bounds were chosen based on the inner and outer bounds of the pSFT mapping stimuli. When considering pSFT parameters, we excluded any voxels with a pSFT R^2 lower than 10% and μ outside the range presented (0.4–5.9 cpd). The μ range was selected based on expected peak preferred SFs from neurophysiological studies (Campbell et al., 1969; De Valois et al., 1982) and previous work using the pSFT model (Aghajari et al., 2020; Ramirez et al., 2025). We employed a broader range of SFs for the stimulus presentation to ensure that we could capture the full tuning function, including the high SF fall off, and obtain reliable estimates of the range of response. We also excluded any voxels with a bandwidth broader than 7 octaves.

Statistical analysis and data visualization. Both pRF and pSFT analysis were conducted in MATLAB as described above. Line fitting for CPF was done in RStudio [R version 4.4.0 (2024–04-24)] using the following packages: *tidyverse* and *minpack.lm* (Wickham et al., 2019; Elzhov et al., 2023). The function "nlsLM" was used to determine the linear regression [least-squares estimates for parameters in the linear regression (Eq. 4)]. Initial parameters were set at $\alpha = 1$ (the rate of change in CPF) and $c_0 = 0$ (baseline CPF) prior to fitting. Model fits were compared using Akaike information criterion (AIC), where lower values indicate better model fit after accounting for model complexity. The significance of the linear increase in the pRF size and logarithmic decrease in preferred SF as a function of eccentricity was evaluated using one-sided t tests on respective slope coefficients (β) across ROI. A nonparametric Kruskal–Wallis test was done to test for differences in parameters across ROI. All data visualization was done using *ggplot2* and *ggpubr* packages (Wickham, 2007; Kassambara, 2017).

Results

To test for scale invariance in the human visual cortex, we measured pRF and pSFT in the early visual cortex. We first confirmed that the pRF size and SF preference varied as a function of eccentricity in V1–V3: in agreement with previous work (Dumoulin and Wandell, 2008; Aghajari et al., 2020), the pRF size linearly increased with eccentricity (Fig. 1*A*; V1, $\beta = 0.07$; $t_{(1451)} = 15.7$; $p < 0.001$; V2, $\beta = 0.12$; $t_{(1009)} = 20.8$; $p < 0.001$; V3, $\beta = 0.133$; $t_{(612)} = 18.2$; $p < 0.001$), while preferred SF decreased logarithmically (Fig. 1*B*; preferred SF = log[eccentricity]; V1, $\beta = -0.58$; $t_{(1451)} = -43.5$; $p < 0.001$; V2, $\beta = -0.47$; $t_{(1009)} = -35.8$; $p < 0.001$; V3, $\beta = -0.34$; $t_{(612)} = -21.3$; $p < 0.001$). Model comparisons based on AIC indicated that the relationship between the pRF size and eccentricity was better explained by a linear (AIC = 1,072.6) compared with a logarithmic model (AIC = 1,258.0). In contrast, SF preference's relationship with eccentricity was better captured by a logarithmic model (AIC = 2,739.2 vs 3,288.8). Despite global patterns of the pRF size and SF tuning across eccentricity, we also observed variability across subpopulations. Specifically, for a given pRF size, we observed a range of SF preferences (μ) and bandwidths (σ). Figure 1*C* demonstrates the distribution of SF tuning as a function of the pRF size, and Supplementary Figure 3 depicts the relationship between bandwidth (σ) and pRF size. Despite the heterogeneity of SF tuning within each pRF size bin, the median of the distributions followed the expected pattern: as the pRF size increased, preferred SF shifted to lower frequencies.

To quantify the spatial information encoded by a pRF, we defined a unifying metric: "CPF." Assuming the relationship between the pRF size and preferred SF is scale-invariant, one would expect CPF to remain constant across eccentricity (Eq. 4) as follows:

$$c = \mu * \sigma = \alpha\rho + c_0, \quad (4)$$

where c is the scaling constant in units of CPF; μ is the preferred SF; σ is the pRF size; α is the rate of change in CPF with pRF eccentricity, ρ; and c_0 is the baseline CPF. We indeed found a constant CPF within V1, V2, and V3, providing evidence for scale invariance in the early visual cortex.

We then considered how CPF changed as a function of the visual area by examining how the slope (α) and intercept (c_0) varied across V1, V2, and V3 for individual participant data (Fig. 2*B*,*C*). When collapsed across all data, we found CPF remained consistent across both eccentricity and visual area (Fig. 2), with a slope of 0.02, 0.08, and 0.13 for V1, V2, and V3, respectively. The intercept was slightly higher in V1 (0.56 CPF) compared with V2 (0.4 CPF) and V3 (0.43 CPF). When considering how CPF varied across individual participants, we found no significant difference across visual areas for both slope and intercept (Kruskal–Wallis, $p = 0.16$ and $p = 0.24$, respectively).

Previous work has highlighted differences in SF tuning across the polar angle (Carrasco et al., 2001; Aghajari et al., 2020; Himmelberg et al., 2023). In line with these findings, we observed expected variations in SF tuning, with higher SF preferences in the horizontal compared with vertical meridian, and in the inferior compared with the superior visual field. However, despite these local differences, our results demonstrate that scale invariance remained consistent across the visual field in V1 and V2. While this pattern was less consistent in V3, this is likely driven by the paucity of voxels in the far periphery (Fig. 3).

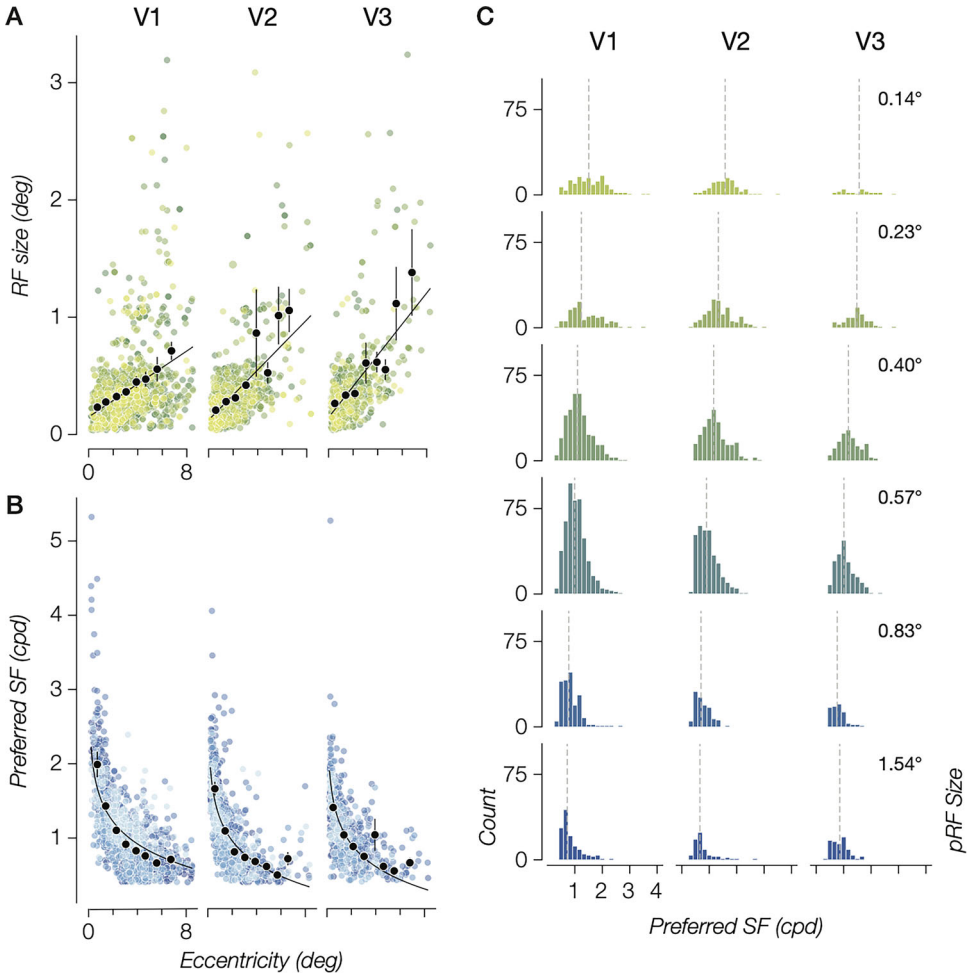

Figure 1. The pRF size and preferred SF scale with eccentricity. ***A***, The pRF size as a function of eccentricity. Individual data points represent voxels; color represents individual participant. The black regression line is fit to all data. Black data points show median value of binned data (for both *x*- and *y*-axes), and confidence intervals show standard error across participants within each bin. Bin boundaries were linearly spaced ($n = 10$) from 0.2 to 8° eccentricity. ***B***, Preferred SF as a function of eccentricity. Individual data points represent voxels; color represents individual participant. The black lines represent a log(X) fit of the collapsed data. Black data points show the median value of binned data, and error bars show standard error across participants within each bin. ***C***, Histogram representing the distribution of SF preferences across six log-spaced pRF size bins across all eight participants.

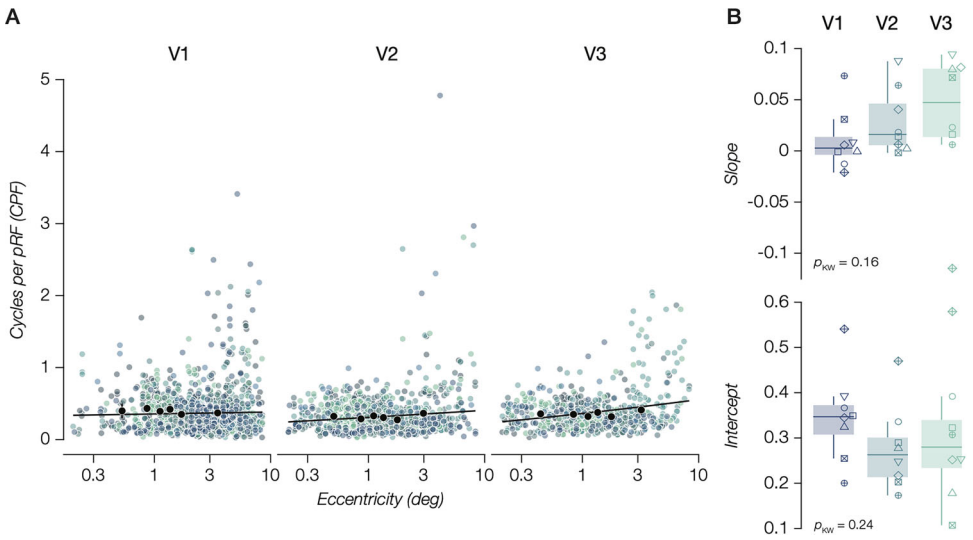

Figure 2. ***A***, CPF as a function of eccentricity. Individual data points represent voxels; color represents individual participants. The black line shows the linear fit (Equation 1) to collapsed data. Black data points show the median value of binned data (for both *x*- and *y*-axes), and error bars indicate the standard error across participants within each bin. Bin boundaries were linearly spaced ($n = 10$) from 0.2 to 8° eccentricity. ***B***, Slope estimate for the linear regression of CPF as a function of eccentricity for individual participants across the visual area. Different participants are indicated by shape. ***C***, Intercept estimates for the linear regression fit for individual participants across the visual area. Different participants are indicated by shape.

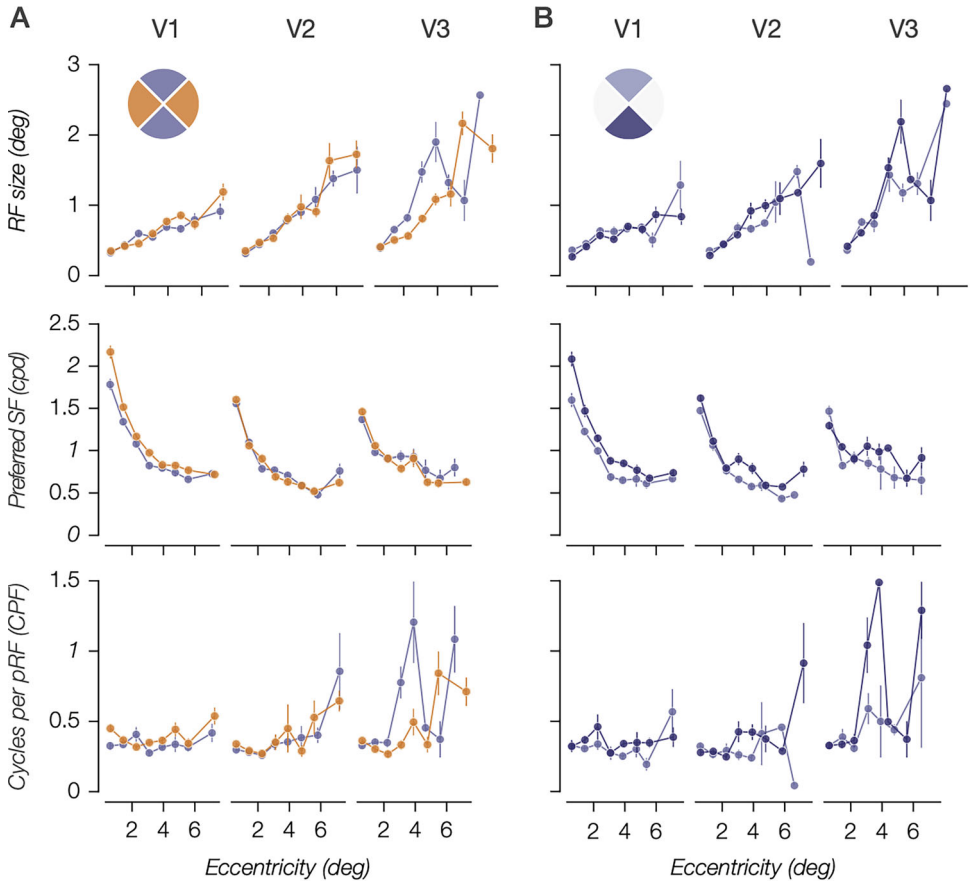

Figure 3. ***A***, The pRF size, preferred SF, and CPF as a function of pRF eccentricity for the horizontal and vertical meridian. Color depicts the meridian based on polar angle estimates from pRF mapping. Data were binned into seven evenly distributed bins from 0.15 to 8° of eccentricity, with one larger bin from 6 to 8° of eccentricity. Error bars depict standard error within each bin. ***B***, The pRF size, preferred SF, and CPF as a function of eccentricity for the superior and inferior visual field. Color depicts the visual field area based on polar angle estimates from pRF mapping. Data were binned into seven evenly distributed bins from 0.15 to 8° of eccentricity, with one larger bin from 6 to 8° of eccentricity. Error bars depict standard error within each bin.

Discussion

The measure of CPF introduced here provides a novel conceptual framework for understanding spatial vision in the context of scale invariance. The metric's utility lies in its independence from physical space, offering a more accurate representation of the resolution of spatial sampling within a unit pRF. Our findings demonstrate that in early visuocortical processing, scale invariance persists across eccentricity, as evidenced by a constant CPF. This reinforces the notion of scale-invariant organization in early areas of the visual hierarchy.

The concept of scale invariance likely applies to multiple levels along the visual hierarchy, from the tuning properties of visual neurons to higher-order pathways involved in processes like object recognition (Teichert et al., 2007; Han et al., 2020). While there is some evidence to suggest that local variability in RF properties may deviate from scale invariance at a neuronal level, Chen et al. demonstrate that this variability can be explained by uniform spatial pooling of inputs, which allows for scale-invariant processing at the population level. Their findings suggest that while individual RFs may exhibit local deviations, population-based measures that integrate these individual properties support the notion of scale invariance in the early visual cortex (Chen et al., 2020). A 2 mm voxel contains on the order of 300,000–500,000 single neurons, and there are inherent differences between single-unit analyses and population-based measures in fMRI (Leuba and Garey, 1989; Sadil et al., 2022). Our findings should be interpreted within this context. Specifically, while pRF estimates largely show correspondence with single-unit RF properties (Keliris et al., 2019; Klink et al., 2021), the linear relationship with eccentricity does not hold over broader ranges (Van Essen et al., 1984). Within an eccentricity range commonly used with fMRI, we find that SF preferences in V1–V3 scale proportionally with the pRF size. This result expands previous work by Broderick et al. that evaluated SF tuning as a function of V1 surface area and found no intrinsic correlation (Broderick et al., 2022). (We also acknowledge that both measures of pRF and pSFT are susceptible to measurement noise. Additionally, we found that fixational eye movements introduce comparable levels of noise in both measures, which is quantitatively assessed in Supplemental Fig. 1.)

Our results also highlight slight differences between horizontal and vertical meridians, as well as between the upper and lower visual fields, in terms of preferred SF. These differences, however, did not persist when comparing CPF. This finding suggests that while there are small topographical variations in SF preference, these do not disrupt the overarching pattern of scale invariance in early cortical areas. This observation aligns with the findings of De Valois et al. (De Valois et al., 1982), who noted variations in SF tuning across different parts of the visual field but emphasized that these differences are often small and do not undermine the concept of a unified visual processing system across the field.

The observed topographical relationship between the RF size and SF preference has motivated vision research to use a constant scalar—the cortical magnification factor—to adjust the size of visual stimuli in a manner that respects the size of its cortical representation. Indeed, this operation is commonly used to equate performance between central and peripheral vision, where computation is performed across sparser, larger, and more overlapping RFs relative to central vision (Rovamo and Virsu, 1979). Despite such widely held assumptions about the anatomical and computational constraints that mediate scale invariance in vision, we lacked validation of whether the resolution of spatial information a pRF encodes is indeed constant across the early visual cortex (Benson et al., 2021). Our work validates this assumption and supports the psychophysical and computational approaches that rely on it (Keliris et al., 2019). Furthermore, our work here established CPF as a unitless metric that may provide a useful framework for characterizing the organization of early vision, particularly in instances where the RF size and SF tuning do not covary as expected. For example, when SF tuning is modulated by attention, CPF could reveal if these changes occur independently of the SF size or, conversely, when pRF is modulated (e.g., by task demands or adaptation), CPF could clarify the consequences for SF tuning (Anton-Erxleben and Carrasco, 2013; Altan et al., 2025; Ramirez et al., 2025). Beyond basic research, CPF may also be useful in identifying atypical visual development. For example, in the case of amblyopia, where there is evidence to suggest that both the RF size and SF tuning have been shown to deviate from typical patterns (Clavagnier et al., 2015), CPF could provide a principled metric to quantify these changes and inform methods to characterize visual deficits in these populations. Specifically, rather than the traditional use of a cortical magnification factor, peripheral visual targets could be scaled by empirically measured CPF to more accurately capture the sampling properties of peripheral RFs.

In conclusion, we define CPF as a measure of visual processing, one that is agnostic to visual–spatial references (i.e., visual degrees). RF and SF tuning are inherently related to one another, and by examining this interdependence through CPF, we can better surmise the first stages of visual processing. Our observation that SF preference scales linearly with the pRF size provides evidence that common assumptions about cortical magnification and spatial processing in early vision are not only valid but fundamental to our understanding of visual processing.

Data Availability

The code and data generated for the paper are available here: https://osf.io/mdkj4/.

References

Aghajari S, Vinke LN, Ling S (2020) Population spatial frequency tuning in human early visual cortex. J Neurophysiol 123:773–785.

Altan E, Morgan CA, Dakin SC, Schwarzkopf DS (2025) Spatial frequency adaptation modulates population receptive field sizes. Elife 13:RP100734.

Andersson JLR, Skare S, Ashburner J (2003) How to correct susceptibility distortions in spin-echo echo-planar images: application to diffusion tensor imaging. Neuroimage 20:870–888.

Anton-Erxleben K, Carrasco M (2013) Attentional enhancement of spatial resolution: linking behavioural and neurophysiological evidence. Nat Rev Neurosci 14:188–200.

Benson NC, Kupers ER, Barbot A, Carrasco M, Winawer J (2021) Cortical magnification in human visual cortex parallels task performance around the visual field. Elife 10:e67685.

Brainard DH (1997) The psychophysics toolbox. Spat Vis 10:433–436.

Broderick WF, Simoncelli EP, Winawer J (2022) Mapping spatial frequency preferences across human primary visual cortex. J Vis 22:3.

Campbell FW, Cooper GF, Enroth-Cugell C (1969) The spatial selectivity of the visual cells of the cat. J Physiol 203:223–235.

Carrasco M, Talgar CP, Cameron EL (2001) Characterizing visual performance fields: effects of transient covert attention, spatial frequency, eccentricity, task and set size. Spat Vis 15:61–75.

Chen Y, Ko H, Zemelman BV, Seidemann E, Nauhaus I (2020) Uniform spatial pooling explains topographic organization and deviation from receptive-field scale invariance in primate V1. Nat Commun 11:6390.

Clavagnier S, Dumoulin SO, Hess RF (2015) Is the cortical deficit in amblyopia due to reduced cortical magnification, loss of neural resolution, or neural disorganization? J Neurosci 35:14740–14755.

De Valois RL, Albrecht DG, Thorell LG (1982) Spatial frequency selectivity of cells in macaque visual cortex. Vision Res 22:545–559.

Dumoulin SO, Wandell BA (2008) Population receptive field estimates in human visual cortex. Neuroimage 39:647–660.

Elzhov TV, Mullen KM, Spiess A-N, Bolker B (2023) minpack.lm: R Interface to the Levenberg-Marquardt Nonlinear Least-Squares Algorithm Found in MINPACK, Plus Support for Bounds. Available at: https://CRAN.R-project.org/package=minpack.lm

Greve DN, Fischl B (2009) Accurate and robust brain image alignment using boundary-based registration. Neuroimage 48:63–72.

Han Y, Roig G, Geiger G, Poggio T (2020) Scale and translation-invariance for novel objects in human vision. Sci Rep 10:1411.

Himmelberg MM, Winawer J, Carrasco M (2023) Polar angle asymmetries in visual perception and neural architecture. Trends Neurosci 46:445–458.

Jamar JH, Koenderink JJ (1983) Sine-wave gratings: scale invariance and spatial integration at suprathreshold contrast. Vision Res 23:805–810.

Kassambara A (2017) ggpubr:"ggplot2" based publication ready plots.

Kay KN, Winawer J, Mezer A, Wandell BA (2013) Compressive spatial summation in human visual cortex. J Neurophysiol 110:481–494.

Keliris GA, Li Q, Papanikolaou A, Logothetis NK, Smirnakis SM (2019) Estimating average single-neuron visual receptive field sizes by fMRI. Proc Natl Acad Sci U S A 116:6425–6434.

Klink PC, Chen X, Vanduffel W, Roelfsema PR (2021) Population receptive fields in nonhuman primates from whole-brain fMRI and large-scale neurophysiology in visual cortex. Elife 10:e67304.

Leuba G, Garey LJ (1989) Comparison of neuronal and glial numerical density in primary and secondary visual cortex of man. Exp Brain Res 77:31–38.

Moeller S, Yacoub E, Olman CA, Auerbach E, Strupp J, Harel N, Uğurbil K (2010) Multiband multislice GE-EPI at 7 tesla, with 16-fold acceleration using partial parallel imaging with application to high spatial and temporal whole-brain fMRI. Magn Reson Med 63:1144–1153.

Ramirez LD, Wang F, Ling S (2025) Attention alters population spatial frequency tuning. J Neurosci 45:e0251252025.

Rovamo J, Virsu V (1979) An estimation and application of the human cortical magnification factor. Exp Brain Res 37:495–510.

Sadil P, Cowell RA, Huber DE (2022) A modeling framework for determining modulation of neural-level tuning from non-invasive human fMRI data. Commun Biol 5:1244.

Silva MF, Brascamp JW, Ferreira S, Castelo-Branco M, Dumoulin SO, Harvey BM (2018) Radial asymmetries in population receptive field size and cortical magnification factor in early visual cortex. Neuroimage 167:41–52.

Teichert T, Wachtler T, Michler F, Gail A, Eckhorn R (2007) Scale-invariance of receptive field properties in primary visual cortex. BMC Neurosci 8:38.

Van der Kouwe AJW, Benner T, Salat DH, Fischl B (2008) Brain morphometry with multiecho MPRAGE. Neuroimage 40:559–569.

Van Essen DC, Newsome WT, Maunsell JHR (1984) The visual field representation in striate cortex of the macaque monkey: asymmetries, anisotropies, and individual variability. Vision Res 24:429–448.

Wickham H (2007) The ggplot package. Available at: http://ftp.uni-bayreuth.de/math/statlib/R/CRAN/doc/packages/ggplot.pdf

Wickham H, et al. (2019) Welcome to the tidyverse. J Open Source Softw 4:1686.

Wiskott L (2006) How Does Our Visual System Achieve Shift and Size Invariance? Available at: [Accessed February 27, 2024].

Xu J, Moeller S, Auerbach EJ, Strupp J, Smith SM, Feinberg DA, Yacoub E, Uğurbil K (2013) Evaluation of slice accelerations using multiband echo planar imaging at 3T. Neuroimage 83:991–1001.